Molecular Dynamics Simulations of Pressure Effects on Hydrophobic Interactions

Tuhin Ghosh,[†] Angel E. García,[‡] and Shekhar Garde*[,†]

Contribution from the Department of Chemical Engineering, Rensselaer Polytechnic Institute, Troy, New York 12180, and Theoretical Division, Los Alamos National Laboratory, Los Alamos, New Mexico 87545

Received February 20, 2001. Revised Manuscript Received August 8, 2001

Abstract: We report results on the pressure effects on hydrophobic interactions obtained from molecular dynamics simulations of aqueous solutions of methanes in water. A wide range of pressures that is relevant to pressure denaturation of proteins is investigated. The characteristic features of water-mediated interactions between hydrophobic solutes are found to be pressure-dependent. In particular, with increasing pressure we find that (1) the solvent-separated configurations in the solute−solute potential of mean force (PMF) are stabilized with respect to the contact configurations; (2) the desolvation barrier increases monotonically with respect to both contact and solvent-separated configurations; (3) the locations of the minima and the barrier move toward shorter separations; and (4) pressure effects are considerably amplified for larger hydrophobic solutes. Together, these observations lend strong support to the picture of the pressure denaturation process proposed previously by Hummer et al. (*Proc. Natl. Acad. Sci. U.S.A.* **1998**, *95*, 1552): with increasing pressure, the transfer of water into protein interior becomes key to the pressure denaturation process, leading to the dissociation of close hydrophobic contacts and subsequent swelling of the hydrophobic protein interior through insertions of water molecules. The pressure dependence of the PMF between larger hydrophobic solutes shows that pressure effects on the interaction between hydrophobic amino acids may be considerably amplified compared to those on the methane−methane PMF.

I. Introduction

Pressure effects on proteins and on physicochemical interactions underlying protein stability have attracted considerable attention in recent years. Experimental and theoretical studies have focused on the structural, thermodynamic, and kinetic aspects of unfolding of proteins upon application of high hydrostatic pressures. Motivation for these studies is derived in part from their direct relevance to many important applications. Pressures of the order of 2000 atm have been shown to be able to dissociate biomolecular complexes, such as antigen−antibody complexes or protein aggregates. Indeed, recent studies demonstrate that pressure can provide an effective yet mild means of recovering proteins bound to biospecific adsorbents[1,2] as well as for separation of proteins in inclusion bodies formed during their overexpression.[3] An understanding of pressure effects on proteins may also be relevant to barophilic adaptation processes.[4] A behavior analogous to pressure denaturation is also observed for the case of hydrogels that undergo an abrupt volume change from a shrunken state to a swollen state at a sufficiently high transition pressure.[5] The dependence of the critical micelle concentration of nonionic surfactants on hydrostatic pressure has been reported recently.[6] Structural transitions that include freezing of surfactant tails at high pressures have been proposed to be of value as templates in nanomaterials synthesis.[7]

From a fundamental perspective, understanding pressure unfolding of proteins in general, and its thermodynamics in particular, presents a significant challenge that was brought to light by Kauzmann more than a decade ago.[8] Kauzmann pointed out that modeling protein unfolding by the commonly used "hydrophobic transfer" model fails almost completely to explain pressure denaturation of proteins. In particular, the volume change upon protein unfolding is found to be positive at low pressures but negative at pressures above 1000−2000 atm,[9−11]whereas the corresponding volume changes observed for the transfer of hydrocarbons into water display opposite behavior.[8,12,13]

Experimental observations indicate that the ensemble of pressure denatured proteins differs significantly from that of heat denatured proteins. Small-angle X-ray scattering,[9] NMR, and Fourier transform infrared (FT-IR) spectroscopy[14,15] experiments show that pressure-denatured proteins are relatively

* To whom correspondence should be addressed: e-mail gardes@rpi.edu.
† Rensselaer Polytechnic Institute.
‡ Los Alamos National Laboratory.

(1) Olson, W. C.; Leung, S. K.; Yarmush, M. L. *Biotechnology* **1989**, *7*, 369.
(2) Sundaram, S.; Roth, C. M.; Yarmush, M. L. *Biotechnol. Prog.* **1998**, *14*, 773.
(3) John, R. J. S.; Carpenter, L. F.; Randolph, T. W. *Proc. Natl. Acad. Sci. U.S.A.* **1999**, *96*, 13029.
(4) Gross, M.; Jaenicke, R. *Eur. J. Biochem.* **1994**, *221*, 617.
(5) Kato, E. *J. Chem. Phys.* **2000**, *113*, 1310.
(6) Lesemann, M.; Thirumoorthy, K.; Kim, Y. J.; Jonas, J.; Paulaitis, M. E. *Langmuir* **1998**, *14*, 5339.
(7) Bossev, D. P.; Paulaitis, M. E.; Kline, S. R. submitted 2001.
(8) Kauzmann, W. *Nature* **1987**, *325*, 763.
(9) Panick, G.; Melissa, R.; Winter, R.; Rapp, G.; Frye, K. J.; Royer, C. A. *J. Mol. Biol.* **1998**, *275*, 389.
(10) Vidugiris, G. J. A.; Markley, J. L.; Royer, C. A. *Biochemistry* **1995**, *34*, 4909.
(11) Desai, G.; Panick, G.; Zein, M.; Winter, R.; Royer, C. A. *J. Mol. Biol.* **1999**, *288*, 461.
(12) Scheraga, H. A. *ACS Symp. Ser.* **1994**, *568*, 360.
(13) Harpaz, Y.; Gerstein, M.; Chothia, C. *Structure* **1994**, *2*, 641.
(14) Inoue, K.; Yamada, H.; Akasaka, K.; Hermann, C.; Kremer, W.; Maurer, T.; Doker, R.; Kalbitzer, H. R. *Nat. Struct. Biol.* **2000**, *7*, 547.

10.1021/ja010446v CCC: $20.00
Published on Web 10/13/2001

compact and retain elements of secondary structure in contrast to the extended, nearly random coil configurations observed for the heat-denatured proteins.[9,16] NMR studies indicate enhanced rates of hydrogen exchange for proteins under high pressures,[17] suggesting disruption of the native state through the insertion of water molecules into the tightly packed hydrophobic core of the protein. A conceptual framework for pressure denaturation that emerges from these studies is a process in which increasing hydrostatic pressure forces water molecules into the protein interior, leading to water-swollen but compact structures for pressure-unfolded proteins.[18]

Using this conceptual framework, Hummer et al. focused on the process of insertion of water into hydrophobic interior of proteins. In particular, they investigated the effect of pressure on the water-mediated interactions between hydrophobic solutes using the information theory approach.[19] They found that the water-separated configurations of hydrophobic solutes become more favorable relative to the contact configurations with increasing pressure. The height of the desolvation barrier between contact and water-separated configurations also increases monotonically with increasing pressure, indicating positive activation volumes and the corresponding slowdown of both the folding and unfolding reactions at higher pressures. Pressure-jump studies on the folding/unfolding of proteins also indicate higher volumes for transition state compared to both the folded and unfolded states.[10] The calculations of Hummer et al. using an information theory (IT) approach are therefore consistent with those obtained from experimental studies of pressure unfolding of proteins. Indeed, the effects of pressure in slowing down the folding/unfolding kinetics of proteins were observed by Hillson et al.[20] in their off-lattice minimalist model simulations. They used a potential energy function among native pairs in a β-barrel protein that mimics qualitatively the pressure-dependent PMF of methane pairs in aqueous solution as described by Hummer et al.[18] They found that pressure affects the participation of contacts in the folding transition state and decreases the chain configurational diffusion, in agreement with experimental data on staphylococcal nuclease.[9]

Pressure effects on association of nonpolar solutes have been the subject of previous molecular simulation studies. In his simulations of concentrated solutions of methanes, Wallqvist found that methanes form aggregates under ambient conditions that are destabilized upon application of high pressures.[21−23] More recently, Payne et al. calculated the pressure dependence of methane−methane potential of mean force (PMF) in water using Monte Carlo simulations.[24] By expressing the change in free energy of association as a function of pressure in terms of first- and second-order terms that involve changes in reaction volume and isothermal compressibility, respectively, they concluded that the volume term favors association at normal pressures while the second-order compressibility term dominates at high pressures, leading to disruption of contact configurations.

Table 1. Isothermal Compressibilities of Pure Water[52]

P, atm	χ_T, 10^{-6} atm^{-1}
1	44.6
2500	29.7
4000	23.5
6000	19.5
8000	15.0

Decrease in the tendency of aggregation was attributed in a recent simulation study to the decreased entropic stabilization of contact configurations at high pressures.[25]

Although results of these simulations are in qualitative agreement with the predictions of information theory,[18] a more quantitative comparison has not been possible due to the lack of definitive results for the pressure dependence of the PMFs between hydrophobic solutes. Here we present such results from long molecular dynamics (MD) simulations of aqueous solutions of methanes over a wide range of pressures relevant to the denaturation of proteins. We quantify pressure effects on hydrophobic interactions between methanes as well as larger hydrophobic solutes. These results lend themselves to direct comparison with the information theory predictions and also extend the microscopic model for pressure effects put forward by Hummer et al. through the inclusion of solute size effects on the pressure dependence of hydrophobic interactions.

II. Simulation Details

MD simulations in NPT ensemble were carried out for a solution of 10 methanes and 508 water molecules with AMBER6.0.[26] The TIP3P model[27] was used to represent water molecules explicitly, whereas methane molecules were represented by a united atom description with Lennard-Jones $\sigma_{Me-Me} = 3.7$ Å and $\epsilon_{Me-Me} = 1.234$ kJ/mol.[28] Solutions of 10 larger hydrophobic solutes with solute−solute $\sigma = 5.0$ Å and $\epsilon = 1.2264$ kJ/mol were also simulated with 508 water molecules. Lorentz−Berthelot mixing rules [$\sigma_{Me-O} = (\sigma_{Me-Me} + \sigma_{O-O})/2$ and $\epsilon_{Me-O} = (\epsilon_{Me-Me}\epsilon_{O-O})^{1/2}$] were used for calculating methane−water Lennard-Jones parameters.[29] Periodic boundary conditions were applied and electrostatic interactions were calculated by the particle mesh Ewald (PME) method[30] with a grid spacing of approximately 0.8 Å. Bonds involving hydrogens were constrained by use of the SHAKE algorithm[31] with a relative geometric tolerance for coordinate resetting of 0.0005 Å. Berendsen's coupling algorithms were used to maintain constant temperature and pressure[32] with the same scaling factor for both the solvent and solutes and with the time constant for heat bath coupling set at 0.5 ps. The pressure for the isothermal−isobaric ensemble was regulated by using a pressure relaxation time of 0.5 ps in Berendsen's algorithm. Simulations of methane−water systems were carried out at pressures of 1, 2500, 4000, 6000, and 8000 atm and a constant temperature of 300 K. Simulations of larger hydrophobic solutes in water were carried out only at pressures of 1 and 8000 atm and at a temperature of 300 K. For a given pressure, the isothermal compressibility of the system that is required in the application of the Berendsen's pressure coupling algorithm was approximated by the compressibility of pure water at the same pressure as shown in Table 1. However, we

(15) Goosens, K.; Smeller, L.; Frank, J.; Heremans, K. *Eur. J. Biochem.* **1996**, *236*, 254.
(16) Pincet, F.; Perez, E.; Belfort, G. *Macromolecules* **1994**, *27*, 3424.
(17) Lasalle, M. W.; Yamada, H.; Akasaka, K. *J. Mol. Biol.* **2000**, *298*, 293.
(18) Hummer, G.; Garde, S.; García, A. E.; Paulaitis, M. E.; Pratt, L. R. *Proc. Natl. Acad. Sci. U.S.A.* **1998**, *95*, 1552.
(19) Hummer, G.; Garde, S.; García, A. E.; Pohorille, A.; Pratt, L. R. *Proc. Natl. Acad. Sci. U.S.A.* **1996**, *93*, 8951.
(20) Hillson, N.; Onuchic, J. N.; García, A. E. *Proc. Natl. Acad. Sci. U.S.A.* **1999**, *96*, 14848.
(21) Wallqvist, A. *J. Chem. Phys.* **1992**, *96*, 1655.
(22) Wallqvist, A. *Chem. Phys. Lett.* **1991**, *182*, 237.
(23) Wallqvist, A. *J. Phys. Chem.* **1991**, *95*, 8921.
(24) Payne, V. A.; Matubayasi, N.; Murphy, L. R.; Levy, R. M. *J. Phys. Chem. B* **1997**, *101*, 2054.
(25) Rick, S. W. *J. Phys. Chem. B* **2000**, *104*, 6884.
(26) Pearlman, D. A.; Case, D. A.; Caldwell, J. W.; Ross, W. S.; Cheatham, T. E.; Debolt, S.; Ferguson, D.; Seibel, G.; Kollman, P. *Comput. Phys. Commun.* **1995**, *91*, 1.
(27) Jorgensen, W. L.; Chandrashekhar, J.; Madura, J. D.; Impey, R. W.; Klein, M. L. *J. Chem. Phys.* **1983**, *79*, 926.
(28) Jorgensen, W. L.; Tirado-Rives, J. *J. Am. Chem. Soc.* **1988**, *110*, 1657.
(29) Allen, M. P.; Tildesley, D. J. *Computer simulation of liquids*; Clarendon Press: Oxford, U.K., 1987.
(30) Darden, T.; York, D.; Pedersen, L. *J. Chem. Phys.* **1993**, *98*, 10089.
(31) Ryckaert, J. P.; Ciccotti, G.; Berendsen, H. J. C. *J. Comput. Phys.* **1977**, *23*, 327.
(32) Berendsen, H. J. C.; Postma, J. P. M.; van Gunsteren, W. F.; DiNola, A.; Haak, J. R. *J. Chem. Phys.* **1984**, *81*, 3684.

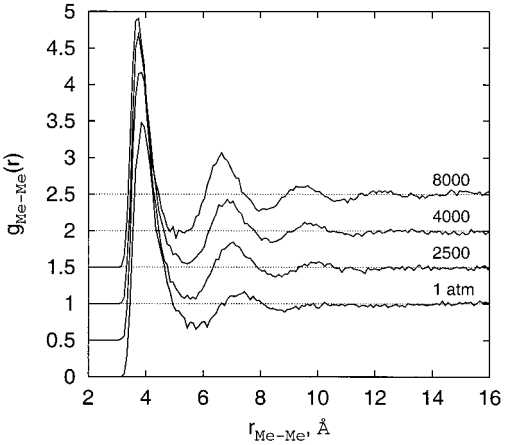

Figure 1. Methane−methane radial distribution functions, $g_{Me-Me}(r)$, obtained from MD simulations at $P = 1$, 2500, 4000, and 8000 atm. The curves have been translated vertically for clarity.

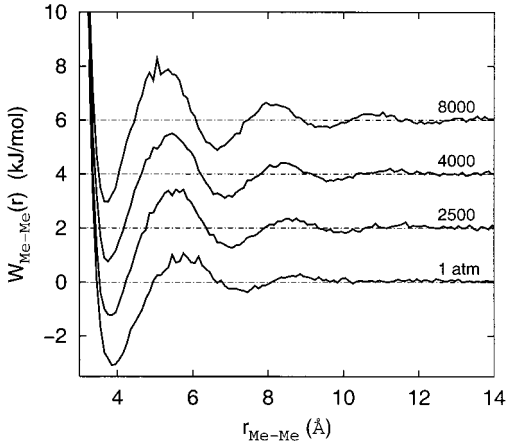

Figure 2. Methane−methane potentials of mean force, $W_{Me-Me}(r) = -kT \ln g(r)$, obtained from $g_{Me-Me}(r)$ shown in Figure 1. The curves have been translated vertically by 2 kJ/mol each beginning with the PMF at 2500 atm.

note that the numerical value of the compressibility does not affect the final equilibrium pressure in a simulation.[32] To get an estimate of the dependence of results on the number of water molecules, we also carried out shorter (1 ns) simulations with twice the number of water molecules at 1 and 8000 atm.

A time step of 2 fs was used in all simulations. Equilibration runs were carried out for 1 ns followed by production runs of 6 ns length. Simulation of 1 ns required approximately 1 day of CPU time on a Compaq XP1000 Alpha processor. In each simulation, a total of 6000 configurations were stored at the frequency of 1/ps during the production runs and were used for further analysis. Statistical errors in the averages were estimated by the method of Flyvbjerg and Petersen.[33] The 6000 configurations were divided initially into $n_b = 40$ blocks of 150 configurations each and the standard deviations were calculated. Changes in standard deviations were then monitored upon application of blocking transformations. The value of the standard deviation for $n_b = 2$ was taken as an estimate of the lower bound for the standard deviation of the data.

The geometry of boxes used for simulations in this work is approximately cubic; the difference in the smallest and the largest box dimensions is less than 2% of the box length. Calculation of the radial distribution functions, $g(r)$, for values of r less than half of the smallest box dimension is straightforward. For larger distances (i.e., regions in the corners of the box), calculation of proper normalization volumes is required. Expressions for proper integrals were evaluated for these normalization volumes for various cases that arise depending on the value of r relative to box dimensions.[34] These normalization volumes were used to calculate radial distribution functions that were further used in the calculation of methane−methane potentials of mean force (PMF), $W(r)$, and the solvent contribution to the methane−methane PMF, $W_{solvt}(r)$, given by

$$W_{solvt}(r) = W(r) - U_{LJ}(r)$$

where $U_{LJ}(r)$ represents the Lennard-Jones potential between united atom methanes.

III. Results and Discussion

A. Methane−Methane Radial Distribution Functions. Figure 1 shows methane−methane radial distribution functions (rdf) in water obtained from MD simulations at four different pressures. The rdf curve at the pressure of 6000 atm was not included in the figure only for visual clarity. Each of these curves shows characteristic features of water-mediated interactions between methanes: at 1 atm pressure, the first peak has a height of approximately 3.5 and appears at a distance of 3.9 Å, corresponding to the direct contact between two methane solutes; a relatively small second peak is observed at a distance of 7.4 Å, corresponding to water-separated configurations of methane pairs in solution. Relatively long production runs and the use of proper normalization volumes in the box corners allow us to calculate the values of $g(r)$ accurately up to distances of 15−16 Å.

With increasing hydrostatic pressure we make the following observations: (1) While the height of the first peak remains approximately constant, the depth of the first minimum and the height of the second peak show significant variations with pressure. In particular, the height of the second peak increases monotonically with increasing pressure, whereas the depth of the first minimum increases with pressure in a similar fashion. (2) We observe an inward movement of location of both the first and the second peaks as well as that of the first minimum with increasing pressure. (3) A distinct third and a weak fourth peak appear at higher pressures, especially at 8000 atm. Similar observations were made when twice the number of water molecules were included in simulations.

B. Pressure Dependence of Methane−Methane PMFs. Figure 2 shows methane−methane PMFs as a function of pressure. At 1 atm, the contact minimum (CM) and the solvent-separated minimum (SSM) are observed at 3.9 and 7.4 Å, respectively, corresponding to the first and second peaks in the Me−Me rdf, whereas the first minimum appears as a desolvation barrier between these minima at 5.8 Å. Since our simulation boxes contain 10 methane solutes, the configuration of two methanes separated by a distance of 7.4 Å can have, in addition to a solvent water molecule, another methane solute nearby. A simple Kirkwood superposition approximation suggests the most favorable location for the third methane to be off-center along the bisector of the methane pair. In what follows, we refer to these water-separated and possibly solute-mediated configurations collectively as SSM.

The pressure dependence of rdfs is reflected in the corresponding PMF profiles. With increasing pressure, the CM is relatively unaffected, whereas the SSM becomes significantly more favorable and the desolvation barrier height increases monotonically with pressure. The inward movement of the CM, the SSM, the desolvation barrier, and the appearance of a third minimum in the PMF are also seen at higher pressures. The values of PMF at the CM, the SSM, and the barrier are reported

(33) Flyvbjerg, H.; Petersen, H. G. *J. Chem. Phys.* **1989**, *91*, 461.
(34) Yang, L.; Garde, S. 2001, private communication.

Table 2. Values of Free Energy[a] at the Contact Minimum (CM), the Solvent-Separated Minimum (SSM), and the Desolvation Barrier (BARR) as a Function of Pressure for Methane−Methane PMFs

P, atm	W_{CM}	W_{SSM}	W_{BARR}
1	−3.097	−0.274	0.889
2500	−3.218	−0.635	1.382
4000	−3.192	−0.753	1.408
6000	−3.328	−0.810	1.571
8000	−3.016	−1.007	1.939

[a] In kilojoules per mole.

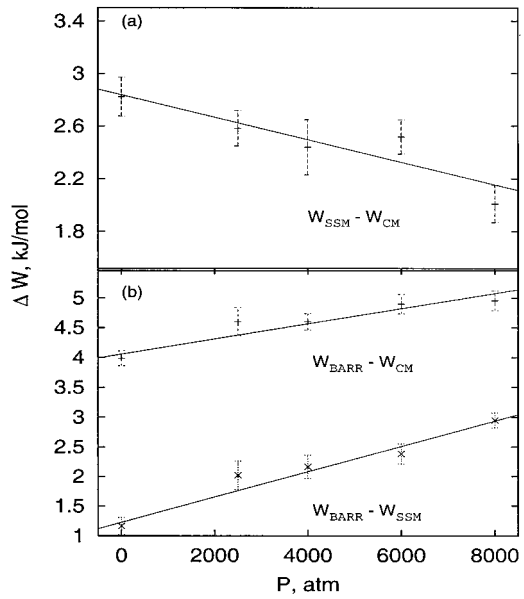

Figure 3. (a) Differences between free energies corresponding to the SSM and the CM, $W_{SSM} - W_{CM}$. (b) Differences between free energies corresponding to the barrier and the CM, $W_{BARR} - W_{CM}$, and between the barrier and the SSM, $W_{BARR} - W_{CM}$, as a function of pressure obtained from MD simulations.

in Table 2. Figure 3a shows the relative stabilization of the SSM in the Me−Me PMF with respect to the CM. In the context of pressure denaturation of proteins, the contact and solvent-separated minima correspond loosely to the hydrophobic contacts in the folded and pressure-unfolded states of proteins, respectively, whereas the desolvation barrier represents partially broken hydrophobic contacts in the dry expanded transition-state ensemble of proteins.[18] With increasing pressure, the free energy corresponding to the SSM decreases linearly with respect to that of the CM. The value of the pressure derivative of this free energy change, $(\partial \Delta W/\partial P)_T = \Delta v_{f\rightarrow u} = -0.85$ mL/mol, represents the contribution to the volume change for each hydrophobic contact broken upon pressure unfolding. At 8000 atm we find that, relative to the PMF difference at 1 atm, the SSM is stabilized by approximately 0.81 kJ/mol (i.e., 0.33*kT*) of free energy with respect to the CM, in excellent agreement with information theory predictions.[18]

The height of the desolvation barrier also increases approximately linearly with respect to both the CM and the SSM as shown in Figure 3b. The pressure derivatives of these free energy changes give activation volumes for the unfolding and folding reactions of $\Delta v_u^{\ddagger} = +1.28$ mL/mol and $\Delta v_f^{\ddagger} = +2.14$ mL/mol, respectively, in good qualitative agreement with the predictions of information theory.[18] The positive activation volumes will lead to slowing down of both the contact formation and breaking reactions, and consequently the folding and unfolding reactions of proteins at high pressures. Experimental results also indicate a considerable slowdown of pressure-induced kinetics of folding and unfolding of proteins with increasing pressure.[10]

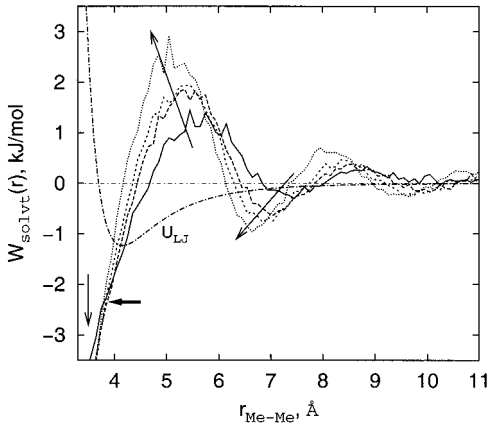

Figure 4. Solvent contributions to the *Me* − *Me* potentials of mean force, $W_{solvt}(r) = -kT \ln g(r) - U_{LJ}(r)$, obtained from MD simulations at $P = 1$, 2500, 4000, and 8000 atm. The curve labeled U_{LJ} is the Lennard-Jones potential for our model methanes ($\sigma = 3.7$ Å, $\epsilon = 1.234$ kJ/mol). Arrows indicate directions of trends with increasing pressure. The bold arrow indicates the point of crossover at about 3.9 Å below which the cavity overlap is stabilized with increasing pressure.

Table 3. Locations of Contact Minimum (CM), Solvent-Separated Minimum (SSM), and the Desolvation Barrier (BARR) between CM and SSM as a Function of Pressure for Methane−Methane PMFs

P, atm	r_{CM}, Å	r_{SSM}, Å	r_{BARR}, Å
1.0	3.93	7.40	5.84
2500	3.88	7.08	5.51
4000	3.86	6.93	5.42
6000	3.76	6.79	5.33
8000	3.74	6.70	5.21

[a] Obtained from local second-order fits.

Figure 4 shows pressure dependence of the solvent contribution to the PMF between a pair of methanes in water. Characteristic features of this curve at atmospheric pressure have been discussed in detail previously.[35−37] The stabilization of the SSM configurations and the destabilization of the desolvation barrier is clearly seen. The key feature in this figure, identified previously by Hummer et al.,[18] is the presence of a configuration or a crossover point at a Me−Me distance of approximately 3.9 Å, the free energy of which is independent of pressure. This results from the opposite effect of pressure on the free energies of the desolvation barrier and the overlapping configurations of methanes. Maintaining the dry volume at the desolvation barrier between two methanes becomes increasingly difficult, whereas free energy for overlapping configurations ($r < 3.9$ Å) that lead to reduced overall volume becomes increasing favorable at higher pressures, which leads to the presence of this crossover point.

C. Pressure Dependence of the Locations of the CM, the SSM, and the Desolvation Barrier. Another feature observed in Figures 2 and 4 is the inward movement of the locations of the CM, the SSM, and the desolvation barrier with increasing pressure. The approximate locations of these minima and the barrier obtained from local quadratic fits to the PMF curves are listed in Table 3. At 8000 atm, the locations of the CM, the barrier, and the SSM move inward by approximately 0.2, 0.6, and 0.7 Å, respectively. As described below, the change in the

(35) Pratt, L. R.; Chandler, D. *J. Chem. Phys.* **1977**, *67*, 3683.
(36) Smith, D. E.; Haymet, A. D. J. *J. Chem. Phys.* **1993**, *98*, 6445.
(37) Garde, S.; Hummer, G.; Paulaitis, M. E. *Faraday Discuss.* **1996**, *103*, 125.

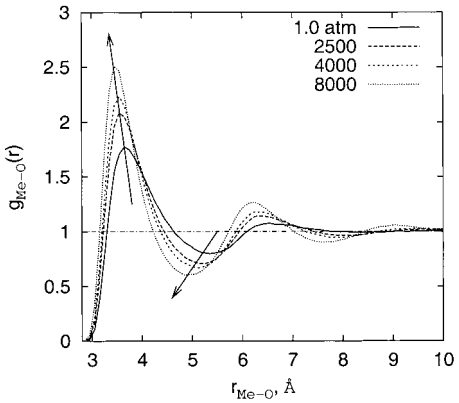

Figure 5. Methane−water oxygen radial distribution functions, $g_{Me-O}(r)$, obtained from MD simulations as a function of pressure. Arrows indicate curves at $P = 1$, 2500, 4000, and 8000 atm.

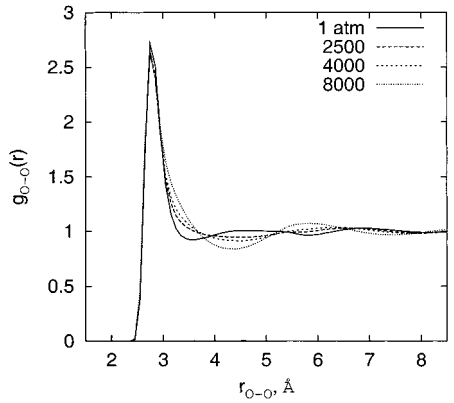

Figure 6. Pair correlation functions for water oxygen atoms, $g_{O-O}(r)$, obtained from MD simulations at $P = 1$, 2500, 4000, and 8000 atm.

exclusion radius of methanes in water accounts only partially for these observations.

Figure 5 shows the methane−water oxygen rdfs as a function of increasing pressure obtained from MD simulations. Consistent with a previous computer simulation study,[38] we observe that heights of both the first and the second peak increase monotonically with increasing pressure, indicating a more efficient packing of water molecules around methanes at higher pressures. The ability to compress the water shell surrounding hydrophobic residues more efficiently relative to the water shells surrounding ionic or polar residues is believed to be an important contributor to negative volumes for unfolding of proteins by pressure.[39,13] In addition, the water exclusion radius of methane, quantified by the smallest distance, r, at which $g_{Me-O}(r) = 1$, decreases from 3.3 Å at 1 atm to 3.15 Å at 8000 atm pressure.

Figure 6 shows the water oxygen−oxygen rdfs as a function of pressure. Changes in water structure with increasing pressure have been investigated previously by molecular simulations[40] as well as by neutron diffraction[41] and X-ray scattering experiments.[42] Changes in the translational and the orientational order in bulk water have also been investigated recently by use of new statistical mechanical methods for quantifying this order.[43] In agreement with previous experimental and simulation

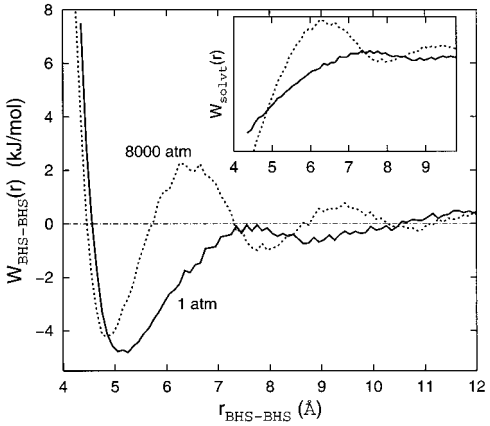

Figure 7. Potentials of mean force between larger hydrophobic solutes (BHS) at pressures of 1 and 8000 atm. The inset shows the solvent contribution to the PMF, $W_{solvt}(r) = -kT \ln g(r) - U_{LJ}(r)$, at $P = 1$ and 8000 atm.

studies, we find that the height and the location of the first peak remains largely unaffected with increasing pressure whereas significant changes are observed in the region $3.0 < r < 7$ Å. In particular, the first peak develops a shoulder between 3 and 3.8 Å and the second peak moves from 4.5 Å to approximately 6.0 Å, indicating changes in the O−O−O triplet correlations and the corresponding tetrahedral coordination of water molecules.

From Figures 5 and 6, we observe a slight reduction (by 0.15 Å at 8000 atm) in water exclusion radius of methane and almost no change in the size of the water molecule itself with increasing pressure. The small inward movement of the CM can be accounted for by the reduction in methane excluded volume; however, the inward movement of the barrier and the SSM by ∼0.6−0.7 Å must result also from changes in the overall water structure as quantified by the pair and higher order water−water correlation functions as a function of pressure. This is clearly seen in the changes in locations of the barrier and the SSM in the solvent contributions to the PMF in Figure 4. Hummer et al. also observed a slight movement of the CM and the barrier and a negligible movement of the SSM in their calculations using the IT approach.[18] However, the much larger shifts in the locations of the minima and the barrier observed in this work could arise primarily from differences in solute−water interactions, hard sphere vs Lennard-Jones, and in part due to differences in the water models, SPC vs TIP3P, employed in the IT calculations and in this work, respectively.

D. Solute Size Effects on Pressure-Dependent Hydrophobic Interactions. Except for alanine, sizes of residues making hydrophobic contacts in the protein interior are greater than the size of methane. For these larger or molecular solutes (e.g., leucine, isoleucine, or valine), pressure effects on hydrophobic interactions are expected to be amplified as the size of the solute increases. Figure 7 shows PMFs between hydrophobic solutes with solute−solute $\sigma = 5$ Å and $\epsilon = 1.2264$ kJ/mol. Thus, these solutes are approximately 35% larger in size compared to methanes. For these larger solutes at 1 atm pressure, we find that the PMF at the contact minimum is −4.7 kJ/mol, significantly lower than the value of −3.1 kJ/mol observed for a pair of methanes (see Table 2). In addition, the behavior at larger solute−solute separations is considerably different: both the desolvation barrier and the SSM are relatively weak, and the water-mediated force of interaction is attractive at even larger distances. The fact that PMF has a positive slope that does not approach a value of 0 at larger separations indicates a strong

(38) Chau, P. L.; Mancera, R. L. *Mol. Phys.* **1999**, *96*, 109.
(39) Kitchen, D. B.; Reed, L. H.; Levy, R. M. *Biochemistry* **1992**, *31*, 10083.
(40) Bagchi, K.; Balasubramaniam, S.; Klein, M. L. *J. Chem. Phys.* **1997**, *107*, 8561.
(41) Soper, A. K. *Chem. Phys.* **2000**, *258*, 121.
(42) Okhulkov, A. V.; Demianets, N.; Gorbaty, E. *J. Chem. Phys.* **1994**, *100*, 1578.
(43) Errington, J. R.; Debenedetti, P. G. *Nature* **2001**, *409*, 318.

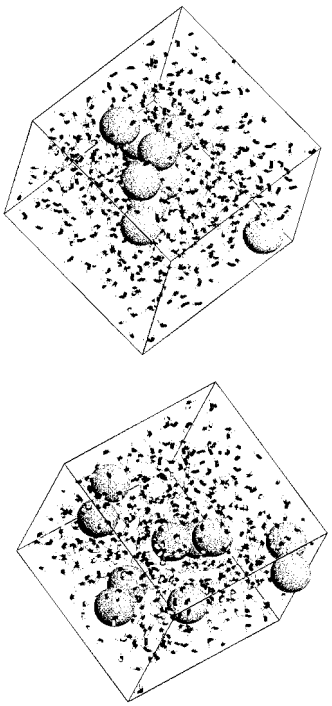

Figure 8. Snapshot from MD simulations of an aqueous solution of 10 hydrophobic solutes with solute−solute Lennard-Jones $\sigma = 5.0$ Å and $\epsilon = 1.2264$ kJ/mol in 508 TIP3P water at 1 atm (top panel) and 8000 atm (bottom panel). Approximately 7−9 solutes at 1 atm aggregate to form a hydrocarbon assembly similar to that observed by Wallqvist.[23] At 8000 atm, the solutes sample contact configurations but no aggregate is observed.

tendency to associate and form aggregates in the system. Long-lived aggregates were indeed observed in simulations at 1 atm as shown in Figure 8 (top). Of 10 large hydrophobic solutes, we found that approximately 7−9 solutes aggregate in a flexible clusterlike configuration that fluctuates with time.

At 8000 atm, the PMF is significantly different from that at 1 atm pressure. Although overall changes are similar to those observed for Me−Me PMFs, they are amplified. The contact minimum shifts inward by about 0.4 Å and is destabilized by 0.7 kJ/mol; the desolvation barrier moves inward by 1.2 Å and increases in height by approximately 2.0 kJ/mol. A significant solvent-separated minimum and a well-developed desolvation barrier appear at 8000 atm pressure. Notable changes occur in the SSM configurations: at 1 atm, the distance of approximately 4 Å between the CM and the SSM indicates a large fraction of solute-separated configurations in the aggregate near the second minimum. However, with increasing pressure, the distance between the CM and the SSM shortens to approximately 3.2 Å, indicating dissociated (i.e., water-separated) configurations at the SSM. Appearance of a second barrier and a third minimum is also clearly observed. Although the net change in $W_{SSM} - W_{CM}$ is only $\sim 0.35kT$, similar to that observed for Me−Me PMF, the significant changes in the overall nature of the PMF, especially those at larger distances, with increasing pressure are sufficient to destabilize and dissolve the long-lived aggregates observed in the simulation at 1 atm. This is also borne out by snapshots from the simulations at the two different pressures in Figure 8; the long-lived aggregate of solutes observed at 1 atm is dissolved at 8000 atm pressure at which a tendency to form contact and solvent-separated pairs is seen without the presence of any long-lived aggregate.

E. Pressure Dependence of Diffusivity of Hydrophobic Solutes. Diffusivities of methanes and larger hydrophobic solutes were calculated from $D = \langle r^2(t)\rangle/6t$, where $\langle r^2(t)\rangle$ is the mean square displacement of a hydrophobic solute at time t from its initial position at time $t = 0$. Diffusivities for water molecules, methanes, and larger hydrophobic solutes obtained from MD simulations are shown in Figure 9 as a function of the system pressure. The water diffusivity and its temperature and pressure dependence have been the focus of recent molecular simulation studies. We find that the numerical value of (TIP3P) water diffusivity is 5.5×10^{-5} cm^2/s at 1 atm and 298 K and decreases monotonically with increasing pressure over the coarse pressure windows (1, 2500, 4000, 6000, and 8000 atm) used here. Mahoney and Jorgensen have reported a quantitative comparison of various water models with regard to their ability of reproducing water diffusivity and its temperature and pressure dependence.[44] Here, we restrict our focus to the pressure dependence of hydrophobic solute diffusivities and its correlation with the observed pressure effects on thermodynamics of hydrophobic interactions.

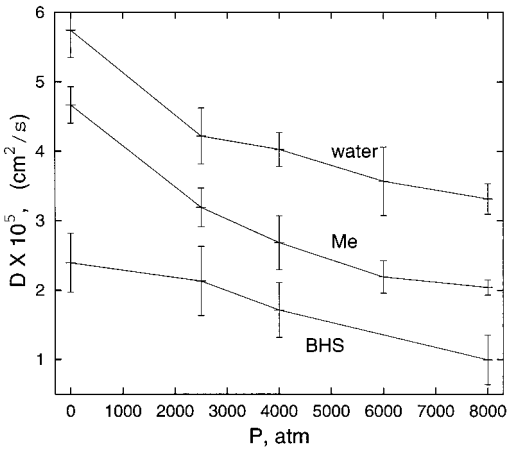

Figure 9. Diffusivities of water molecules, methanes (Me), and larger hydrophobic solutes (BHS) in aqueous solution as a function of pressure obtained from MD simulations. The diffusivities for the larger hydrophobic solutes at the two intermediate pressures of 2500 and 4000 atm were obtained from shorter simulations spanning 2 ns each. Lines are to guide the eye.

For hydrophobic solutes, in particular for larger ones, two opposing factors are expected to influence the dependence of their diffusivity on the system pressure. With increasing pressure, the reduction in free volume in a condensed liquid is expected to reduce the diffusivity, whereas dissociation of close hydrophobic contacts and clusterlike configurations is expected to increase the solute diffusivity. Figure 9 shows, however, that the reduction in free volume dominates the pressure dependence of diffusivity for methanes as well as for larger hydrophobic solutes, leading to a monotonic reduction in diffusivities over the pressure range considered here. The reduction in solute diffusivities with increasing pressure observed here is consistent with a slowdown in contact formation and breakage processes as well as with reduced translational and rotational diffusion of macromolecules at higher pressures.[45] In particular, we find that the solute diffusivities can be correlated with the free energy difference, $W_{Barr} - W_{CM}$, between barrier and contact solute configurations as $D \sim \exp[-(W_{Barr} - W_{CM})/kT]$. If opening of a cavity near the solute by random thermal fluctuations is an important first step in the solute diffusion process, then such a correlation is reasonable; the difference $W_{Barr} - W_{CM}$ gives primarily the free energy of opening a dry volume between two

(44) Mahoney, M. W.; Jorgensen, W. L. *J. Chem. Phys.* **2001**, *114*, 363.
(45) Orekhov, V. Y.; Dubovski, P. V.; Yamada, H.; Akasaka, K.; Arseniev, A. S. *J. Biomol. NMR* **2000**, *17*, 257.

hydrophobic solutes upon going from contact to barrier configuration. More work along these lines is needed, however, before the pressure dependence of diffusion coefficients can be quantitatively related to structural changes in the system.[46]

IV. Conclusions

Understanding effects of environmental variables (e.g., *T* and *P*) on water-mediated interactions between simple hydrophobic solutes has provided important insights into various aspects of the protein denaturation processes.[18,47] In this work, we have used classical MD simulations of aqueous solutions of hydrophobic solutes to quantify the pressure effects on hydrophobic interactions. Our calculations stress the role of hydrophobic interactions in providing thermodynamic stability to folded proteins. We make the following important observations: (1) With increasing hydrostatic pressure, the water-separated configurations of hydrophobic solutes are stabilized with respect to the contact configurations; (2) the height of the desolvation barrier in the Me−Me PMF increases monotonically with respect to both the contact and solvent-separated configurations; (3) the locations of contact and solvent-separated minima and the desolvation barrier move to smaller Me−Me distances with increasing pressure; and (4) although qualitatively similar, the changes in solute−solute PMF are considerably amplified with increasing solute size. Together, these observations lend strong support to the picture of the pressure denaturation process proposed previously by Hummer et al.[18] with increasing pressure, the transfer of water into protein interior becomes key to the pressure denaturation process, leading to the dissociation of close hydrophobic contacts and subsequent swelling of the hydrophobic protein interior through insertions of water molecules.

The excellent agreement between results of all-atom MD simulations presented here and the predictions of IT approach[18,19] underscore the value of IT as a powerful and efficient tool for studies of water-mediated interactions between solutes in a variety of environments. Clearly, changes in water structure quantified by the water oxygen−oxygen radial distribution function as a function of the thermodynamic variable of interest (pressure in the present case) contain valuable information in this regard. Previous studies have shown that changes in water structure quantified by the HH correlation function upon addition of salts are similar to those observed upon increasing the hydrostatic pressure.[48] However, further studies are required to investigate whether these similar structural changes in water also lead to similar changes in hydrophobic interactions in these disparate situations.[49]

Further physical insights into pressure effects observed here will also require understanding of entropic and enthalpic contributions to solute−solute PMFs as a function of pressure. It is well-known that the positive entropy of water molecules that are released into solution upon association of hydrophobic solutes stabilizes the contact minimum, whereas the solvent-separated configurations are enthalpically stabilized.[36,37] Recent calculations by Rick indicate that the entropic contribution becomes less important at higher pressures.[25] However, these observations have not been related so far to the structural details of the CM, the barrier, and the SSM configurations. Quantification of methane−methane−water and methane−methane−methane triplet correlation functions at these configurations with increasing pressure may provide a better understanding of pressure effects on water-mediated interactions between hydrophobic solutes.

Results of the MD simulations of solutions of larger hydrophobic solutes presented here underscore the solute size as an important parameter that affects the solvent-mediated interactions significantly. For larger solutes considered here, although the qualitative picture remains similar to that observed for smaller solutes, the pressure effects on the PMF are amplified significantly. Further, although observations similar to the ones presented here were made from our simulations with twice the number of waters, a systematic study of concentration and solute size-dependent aggregation of hydrophobic solutes may be useful. For example, it is not clear whether observations made here hold true for mesoscopic hydrophobic solutes or a completely different physical picture needs to be considered in such cases.[50] Radius of curvature for larger hydrophobic solutes considered here is comparable in size to the radii of curvature of hydrophobic amino acid side chains. Thus, pressure effects on their PMF in water are directly relevant to pressure denaturation of proteins.

Although the qualitative picture that emerges from the pressure effects on interactions of hydrophobic solutes in water captures the physics of the problem, quantitative understanding of protein denaturation at high pressures will require modeling of more realistic systems. One solution may be to perform large-scale simulations of aqueous protein systems under higher pressures. A few MD simulations of proteins in water at high pressures have been reported previously.[39,51]However, their scope is severely restricted due to unfolding time scales involved in pressure denaturation process that are orders of magnitude longer than what is currently accessible to brute force all-atom MD simulations. Clearly, novel methodological improvements are needed before pressure denaturation of proteins can be observed through molecular simulations.

Acknowledgment. We gratefully acknowledge Drs. G. Hummer, L. R. Pratt, Henry Ashbaugh, and M. E. Paulaitis for many fruitful discussions over the past several years.

JA010446V

(46) Dzugutov, M. *Nature* **1996**, *381*, 137.
(47) Garde, S.; Hummer, G.; García, A. E.; Paulaitis, M. E.; Pratt, L. R. *Phys. Rev. Lett.* **1996**, *77*, 4966.
(48) Leberman, R.; Soper, A. K. *Nature* **1995**, *378*, 364.
(49) Bulone, D.; Martorana, V.; Biagio, P. L. S.; Palma-Vittorelli, M. B. *Phys. Rev. E* **2000**, *62*, 6799.
(50) Lum, K. A.; Chandler, D.; Weeks, J. D. *J. Phys. Chem. B* **1999**, *103*, 4570.
(51) Paci, E.; Marchi, M. *Proc. Natl. Acad. Sci. U.S.A.* **1996**, *93*, 11609.
(52) Hobbs, P. V. *Ice Physics*; Clarendon Press: Oxford, U.K., 1974.